
Article:
Lyu, S., Yang, H., Lin, H. et al. (3 more authors) (2019) Influence of design parameters on on-load demagnetization characteristics of switched flux hybrid magnet memory machine. IEEE Transactions on Magnetics, 55 (7). 8106405. ISSN 0018-9464

https://doi.org/10.1109/tmag.2019.2903160

Influence of Design Parameters on On-Load Demagnetization Characteristics of Switched Flux Hybrid Magnet Memory Machine

Shukang Lyu[1], Hui Yang[1], Heyun Lin[1], Z. Q. Zhu[2], *Fellow, IEEE*, Hao Zheng[1], and Zhenbao Pan[1]

[1]School of Electrical Engineering, Southeast University, Nanjing 210096, China
[2]Department of Electronic and Electrical Engineering, The University of Sheffield, Sheffield S1 3JD, U.K.

In this paper, the influences of design parameters on the on-load demagnetization behavior of a switched flux hybrid magnet memory machine (SF-HMMM) are evaluated, which aims to provide a useful design guideline to avoid this performance degradation. The machine topology and on-load demagnetization phenomenon are described, respectively. Furthermore, some key design parameters are selected to optimize to elevate the operating point of the low coercive force (LCF) permanent magnets (PMs). Then, some geometric modifications are suggested to alleviate the on-load demagnetization effects. Finally, an SF-HMMM prototype is fabricated and tested to experimentally verify the finite-element analysis.

Index Terms— **Hybrid permanent magnet (PM), hysteresis model, memory machine (MM), on-load demagnetization, variable flux.**

I. Introduction

FOR memory machines (MMs) [1]–[19], the magnetically vulnerable low coercive force (LCF) magnets can be purposely utilized to enable flexible air-gap flux adjustment due to their nonlinear hysteresis characteristics. Since the LCF magnets can be magnetized or demagnetized by applying a transient current pulse, the associated excited loss can be neglected. MMs are regarded as a competent candidate for automotive drives with high efficiency across a wide speed range [2].

Based on the magnetizing winding type, MMs can be generally categorized into alternating current (ac) [1]–[9] and direct current (dc) types [10]–[19]. The former is normally characterized by an interior permanent magnet (PM) configuration. However, the usage of LCF PMs makes MMs confront severe demagnetization risks. The demagnetization issues incurred by the q-axis armature reaction are inevitable. In that case, the online magnetization control becomes unpredictable under ac vector control. In order to seek a better design of MM, there is tradeoff between the reduction of the current pulse magnitude for magnetization state manipulation and the improvement of the on-load demagnetization withstand capability. The magnet temperature effect [8] and the PM configuration [9] have remarkable impacts on the magnetization characteristics of the LCF PMs in ac-type MMs.

For the dc-type MMs, the switched flux (SF) structures were recently extended to MMs [15]–[19], which exhibit convenient online magnetization control, thermal management, and rotor robustness. Although the armature reaction and LCF PM fields are parallel, the possibility of unexpected demagnetization may still exist particularly under on-load operation [14], [19]. This is mainly attributed to the magnetic susceptibility of LCF PMs and severe localized magnetic saturation caused by hybrid magnets and armature reaction within the stator. In this case, the resultant magnetic circuit distortion will potentially pose the demagnetization risk for LCF PMs. In addition, this kind of demagnetization is adverse to the on-load dynamic performance as well as the accurate online magnetization control. Hitherto, there are few references on the influences of design parameters on the on-load demagnetization of SF hybrid magnet MM (SF-HMMM), and no general design guideline has been established to improve the on-load demagnetization resist capability.

In this paper, the influences of design parameters on on-load demagnetization characteristics of the SF-HMMM are analyzed in this paper. The main content of this paper can be described as follows. The machine topology and the on-load demagnetization effect of the investigated SF-HMMM are introduced and unveiled in Section II. In Section III, the influences of key design parameters on the demagnetization behaviors of the SF-HMMM are analyzed with the aid of the finite-element analysis (FEA) and frozen permeability method [20]. In addition, in Section IV, some geometric modifications are suggested to alleviate the on-load demagnetization effect of the SF-HMMM. With the guidance of the design parameters analysis, an SF-HMMM prototype is designed and manufactured. The experimental results of the prototype machine are presented in Section V, followed by a comprehensive conclusion in Section VI.

II. Machine Topology and On-Load Demagnetization Effects

The topology of the investigated SF-HMMM with 6-/13-pole configuration is shown in Fig. 1 [16]–[18]. The tangentially magnetized NdFeB PMs are inserted into the stator teeth and the inner part of the stator is divided into six "U"-shaped iron segments. The radially magnetized LCF PMs

Manuscript received November 5, 2018; revised February 14, 2019 and February 14, 2019; accepted February 26, 2019. Corresponding author: H. Yang (e-mail: huiyang@seu.edu.cn).

Color versions of one or more of the figures in this paper are available online at http://ieeexplore.ieee.org.

Digital Object Identifier 10.1109/TMAG.2019.2903160

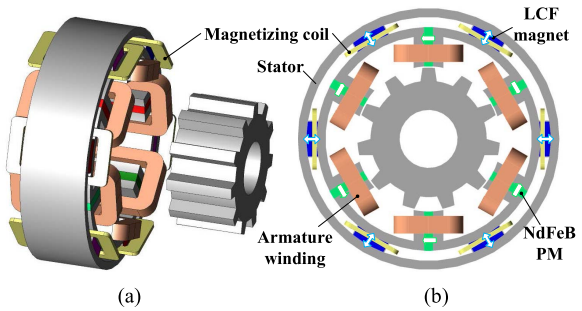

Fig. 1. Topology of the investigated SF-HMMM. (a) 3-D exploded view. (b) Cross-sectional view.

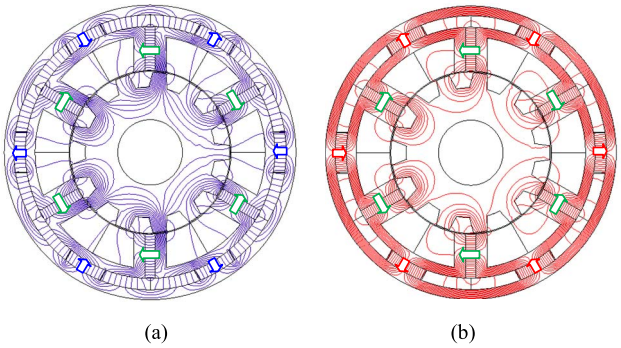

Fig. 2. Open-circuit field distributions of SF-HMMM. (a) Flux enhanced. (b) Flux weakened.

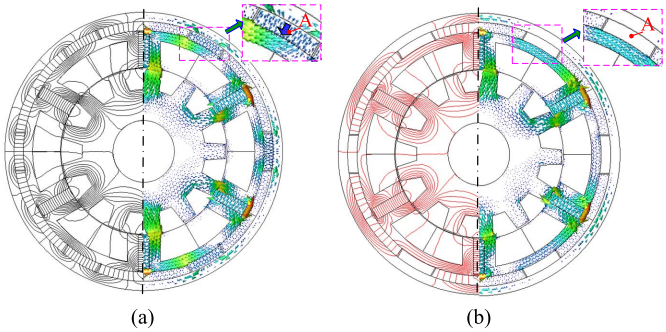

Fig. 3. On-load demagnetization effect: open-circuit field distributions. (a) Before or (b) after the q-axis current excitation ($i_q = 40$ A).

TABLE I
OPTIMIZED DESIGN PARAMETERS OF SIX-STATOR POLE SF-HMMM WITH VARIOUS ROTOR POLE NUMBERS

Item	Value	
Rotor pole number	5/7	11/13
Outer diameter of stator (mm)	90	
Rated speed (r/min)	400	
Split ratio	0.55	0.58
Air-gap length (mm)	0.5	
Active stack length	25	
Stator tooth width (mm)	5	3.2
Ratio of rotor pole to pitch	0.33	
Turns of stator winding per phase	72	84
Turns of per magnetizing coil	100	
NdFeB magnet grade	N35H	
LCF magnet grade	SmCo series-SB12B	

are amounted between the outer stator ring and the "U"-shaped stator segments. The magnetization states and polarities of the LCF PMs can be changed by applying dc current pulses fed by the magnetizing coils wound around the LCF PMs. According to the magnetization direction of the LCF PMs, the SF-HMMM is able to operate at the flux-enhanced state or the flux-weakened state. The resultant flexible air-gap flux adjustment enables the machine to operate over a wide speed range with a high efficiency. When the machine operates at flux-enhanced state, LCF PMs are magnetized as shown in Fig. 2(a) to enhance the air-gap field. On the other side, when it operates at flux-weakened state, LCF PMs are magnetized as shown in Fig. 2(b) to partially short-circuit the NdFeB PM field, resulting in the air-gap flux weakening effect. However, the risk of the on-load demagnetization exists due to the utilization of LCF PMs of the developed machine. The open-circuit field distributions of the machine at flux-enhanced and flux-weakened states are shown in Fig. 2(a) and (b), respectively. It should be pointed out that, for the instance of the investigated SF-HMMM, the LCF PM demagnetization caused by the armature reaction can be avoided at flux-weakened state. In this case, PMs in the stator will form a short-circuit flux loop and the magnetizing state of LCF PMs will be stabilized by NdFeB PMs and armature flux will enter the stator teeth and air gap instead of the saturated parts. Therefore, only the flux-enhanced cases of the SF-HMMM are discussed in this paper.

Due to the effect of cross-coupling demagnetizing [19], the PM flux linkage is a function of i_d and i_q, and the electromagnetic torque T_e of SF-HMMM can be described as

$$T_e = 1.5p[\psi_{\mathrm{PM}}(i_d, i_q)i_q + (L_d - L_q)i_d i_q] \tag{1}$$

where p denotes the machine pole pairs, ψ_{PM} is the flux linkage of PMs, i_d and i_q are the d-axis and q-axis currents, and L_d and L_q are the d-axis and q-axis inductances. Fig. 3 shows the open-circuit field distributions at the flux-enhanced state before or after i_q excitation. The LCF PMs are demagnetized conspicuously during the on-load operation. To maintain the torque performance of the SF-HMMM, the investigation of the effects of design parameters on the demagnetization resistant capability improvement should be carried out. This paper concentrates on the six-stator pole SF-HMMMs as a base machine, and the general design rules can be extended to cover all the cases with higher stator poles. The major design parameters of SF-HMMM with different rotor pole numbers are optimized as listed in Table I as a benchmark to conduct the following analysis. The following analyses aim to reveal the influences of various design parameters on the on-load demagnetization effects of LCF PMs. Based on this, some basic design guidelines will be established.

III. INFLUENCE OF KEY DESIGN PARAMETERS ON DEMAGNETIZATION BEHAVIORS

It should be noted that the LCF PMs are kept constant first because it is obvious that more usage of LCF magnets

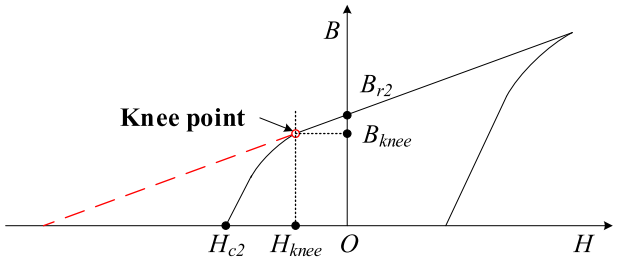

Fig. 4. Hysteresis curve of LCF PMs.

will enhance its on-load demagnetization withstand capability. As a result, only parts of the key parameters are added for illustrating their influences on the on-load demagnetization withstand capability. As spilt ratio of the machine increases, the slot area and lengths of NdFeB PMs decrease. Therefore, the demagnetization field is weakened and the working points of LCF PMs are elevated. In addition, the increase of the rotor pole number and rotor pole width will intensify the flux leakage of NdFeB PMs, and hence, the working points of LCF PMs are increased. On the other hand, as the NdFeB PM thickness is increased, the working points of LCF PMs of the machine at flux-enhanced state are reduced. Based on the discussion above, an FEA method is utilized to evaluate the effect of these parameters on the on-load demagnetization of the SF-HMMM. The rotor pole number can be chosen close to the multiples of the stator pole number, i.e., 5, 7, 11, and 13 so as to obtain high winding factor [21]. Then, a comprehensive investigation is conducted to disclose how and why the dominant sensitive parameters influence the demagnetization behaviors. The LCF PM coercive forces are set as −200 kA/m in advance. To estimate whether the on-load demagnetization happens, the working point is compared to the knee point as shown in Fig. 4. The characteristics of the LCF PMs can be regarded as the extended line of the upper recoil line, which can be expressed as [14]

$$B = B_{\text{rknee}} + \mu_0 \mu_{r2}(H - H_{\text{knee}}) \tag{2}$$

where μ_0 and μ_{r2} are the vacuum and LCF PM relative permeability, B_{rknee} and H_{knee} are the residual flux density and magnetic field intensity of the knee point. The variation of LCF working flux density is utilized to quantitatively reflect the on-load demagnetization effects.

For SF-HMMMs with different rotor teeth, the average flux densities of LCF PMs before or after loaded operation as functions of various design parameters are illustrated in Fig. 4. Overall, the SF-HMMMs with higher rotor tooth numbers have better on-load demagnetization withstand capability than their low-rotor tooth counterparts. To evaluate the on-load demagnetization withstand capability $k_{\text{on-load}}$ is defined as follows:

$$k_{\text{on-load}} = \frac{M_{iq} E_1}{E_1 - E_2} \tag{3}$$

where M_{iq} is the magnitude of the q-axis current excitation, E_1 and E_2 are the back electromotive force (EMF) magnitudes before and after i_q excitation. The reduction of rare-earth usage

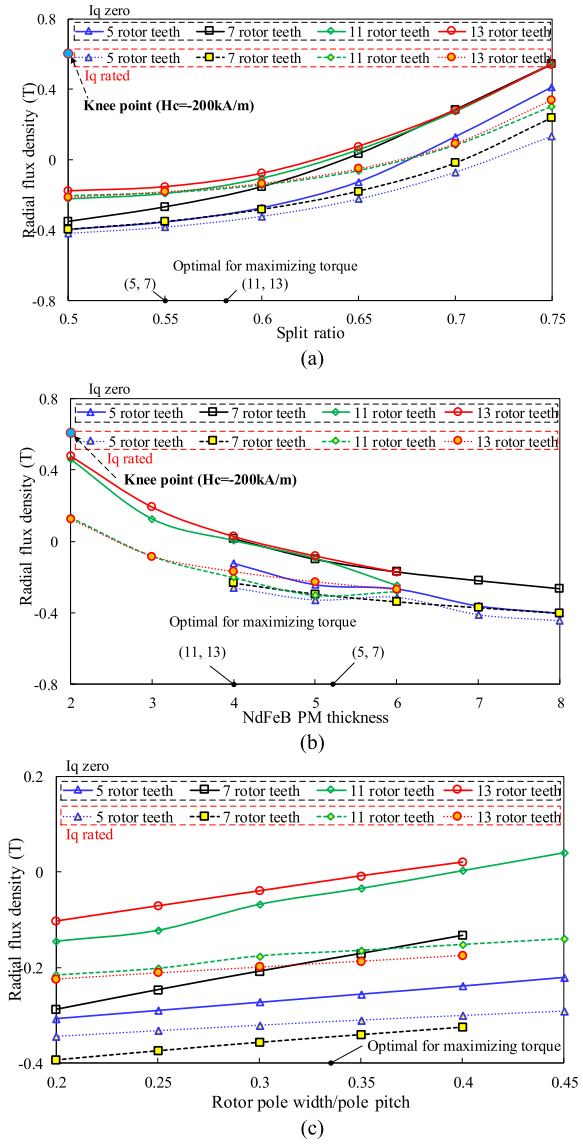

Fig. 5. Variation of working flux densities of point *A* with various parameters in SF-HMMM with different rotor teeth. (a) Split ratio. (b) NdFeB thickness. (c) Rotor pole width.

and larger air-gap permeance is responsible for this phenomenon. Consequently, the operating points of LCF magnets are correspondingly elevated. In addition, in Fig. 5(a), it can be observed that the increase of split ratio can elevate the working points of LCF PMs. However, the on-load demagnetization appears to be aggravated. It implies that the higher the working points the lesser the required demagnetization MMF due to the hysteresis characteristics.

Fig. 5(b) shows that the on-load demagnetization increases with the NdFeB thickness as anticipated, whereas the on-load demagnetization effects are slightly alleviated with the increment of NdFeB thickness. Meanwhile, it can be seen from Fig. 5(c) that the on-load demagnetization can be alleviated by increasing the rotor pole width due to the larger circulating permeance within the stator/rotor aligning parts. The 6-/13-pole SF-HMMM is chosen for the following analysis due to not only the desired torque capability [19] but also the advantageous demagnetization withstand capability.

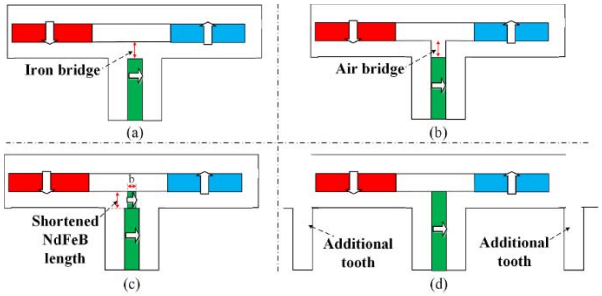

Fig. 6. Effective modified geometry for resisting the on-load demagnetization. (a) Iron bridge. (b) Air bridge. (c) Segmented unequal NdFeB PMs. (d) E-core.

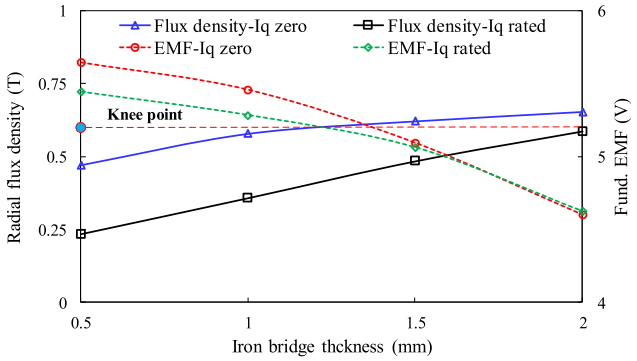

Fig. 7. Variation of working flux density and fundamental back-EMF values with various iron bridge thicknesses.

IV. Geometric Modifications for Demagnetization Withstand Ability Enhancement

In order to ameliorate the demagnetization effect of variable flux LCF PMs in SF-HMMMs, some geometric modification methods are suggested and illustrated in Fig. 6. The most straightforward way is to widen the iron bridge attached to the upper side of NdFeB PM, which can alleviate the magnetic saturation. Fig. 7 shows the variations of LCF PM working flux densities ($H_{c2} = -200$ kA/m and $h_{m2} = 3$ mm) and fundamental EMF values with the iron bridge thickness. It implies that the on-load demagnetization can be effectively attenuated with the increase of iron bridge thickness. However, the back-EMF magnitudes are reduced due to the short-circuiting of the NdFeB flux within the bridge.

Alternatively, when removing the iron bridge, namely, an air bridge is placed instead as shown in Fig. 6(b). The LCF PM working points and fundamental EMF values as functions of air bridge thickness are shown in Fig. 8. It can be observed that the working points increase at the cost of the EMF reduction. Similarly, when inserting small amount of NdFeB PMs into the iron bridge, the variation of the working point with width and length of the shortened NdFeB segment is shown in Fig. 9. The working points and back EMFs keep almost constant as long as the length proportion between two separate NdFeB segments is fixed. It indicates that the demagnetization effect is dominantly sensitive to the cross-sectional areas of NdFeB PMs. It is worth noting that the back-EMF loss can be well compensated compared with the iron bridge cases albeit with slight compromise in on-load demagnetization capability.

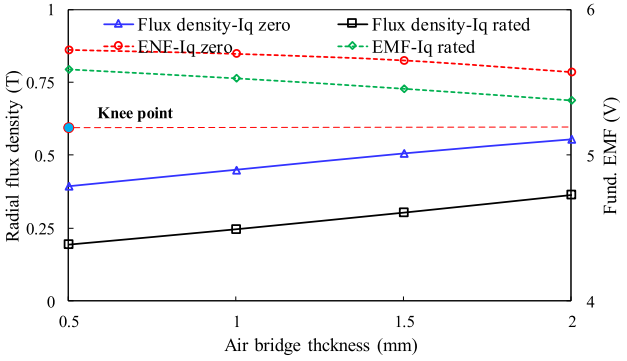

Fig. 8. Variation of working flux density and fundamental back-EMF values with air bridge thickness.

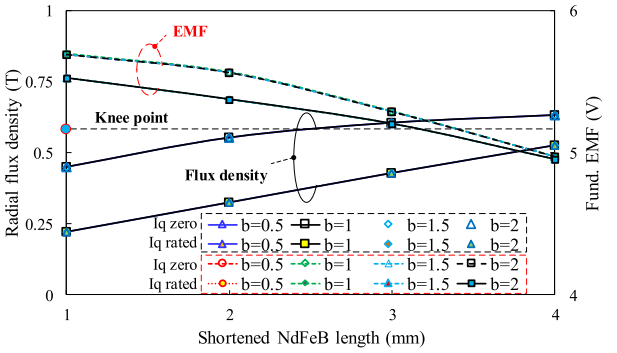

Fig. 9. Variation of working flux density and fundamental back-EMF values with shortened NdFeB length and width.

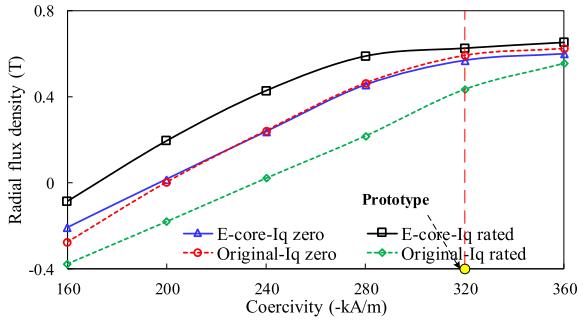

Fig. 10. Working flux densities as a function of LCF magnet coercivity with reference to E-core and original cases.

Finally, the additional intermediate stator teeth can be designated to form an E-core structure, which can allow the effective circulating paths for strong NdFeB/armature fields. The working point as a function of LCF PM coercivity is calculated and compared with the original results (C-core) as shown in Fig. 10. It can be seen that both the on-load demagnetization withstand capabilities are enhanced particularly in the high coercive force cases. Thus, the effectiveness of this geometric modified approach is verified.

V. Experimental Validation

An SF-HMMM prototype with 6-/13-pole configuration is manufactured and tested to verify the foregoing theoretical analyses. The stator and rotor assemblies of the SF-HMMM

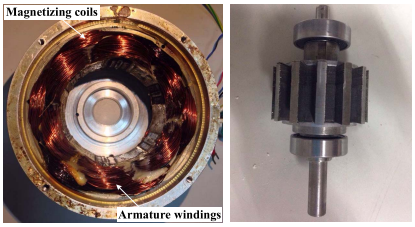

(a) (b)

Fig. 11. 6-/13-pole SF-HMMM prototype. (a) Stator assembly. (b) Rotor assembly.

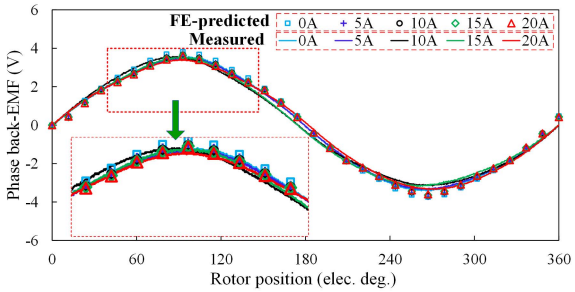

Fig. 12. Comparison of finite element predicted and measured open-circuit back-EMF characteristics before and after i_q excitation, 300 r/min.

are shown in Fig. 11(a) and (b), respectively. Fig. 12 shows the measured open-circuit back EMF before and after different magnitudes of i_q. It can be seen that the drop of back EMF after i_q excitation is inconspicuous, which indicates that the magnetization states of LCF magnets are well maintained. Overall, the SF-HMMM prototype shows a good capability to resist the on-load demagnetization, which confirms the effectiveness of the abovementioned parameter influences analysis.

VI. Conclusion

In this paper, the influences of various parameters on the on-load demagnetization effect of the studied machine are evaluated. It shows that the SF-HMMM having higher rotor pole numbers have better on-load demagnetization withstand capability than their low-rotor pole counterparts due to higher working points of LCF PMs. Meanwhile, the on-load demagnetization can be alleviated with the increase of split ratio, the decrease of NdFeB thickness, and widening rotor pole width. Some design modification suggestions for preventing the undesired demagnetization are provided. It can be found that the on-load demagnetization withstand the capability of SF-HMMM is improved by inserting small amount of NdFeB PMs into the iron bridge and the utilization of E-core structure. The theoretical analyses are validated by the experimental tests on a 6-/13-pole SF-HMMM prototype.

Acknowledgment

This work was jointly supported in part by National Natural Science Foundations of China under Grant 51377020 and 51377036, in part by Natural Science Foundation of Jiangsu Province for Youth (BK20170674), in part by the Fundamental Research Funds for the Central Universities (2242017K41003), in part by "Hong Kong Scholar" Program (XJ2018014), in part by Supported by the "Excellent Young Scholars" Program of Southeast University, and in part the Scientific Research Foundation of Graduate School of Southeast University.

References

[1] V. Ostovic, "Memory motors," *IEEE Ind. Appl. Mag.*, vol. 9, no. 1, pp. 52–61, Jan./Feb. 2003.
[2] N. Limsuwan, T. Kato, K. Akatsu, and R. D. Lorenz, "Design and evaluation of a variable-flux flux-intensifying interior permanent-magnet machine," *IEEE Trans. Ind. Appl.*, vol. 50, no. 2, pp. 1015–1024, Mar./Apr. 2014.
[3] H. Liu, H. Lin, Z. Q. Zhu, M. Huang, and P. Jin, "Permanent magnet remagnetizing physics of a variable flux memory motor," *IEEE Trans. Magn.*, vol. 46, no. 6, pp. 1679–1682, Jun. 2010.
[4] S. Maekawa *et al.*, "Study of the magnetization method suitable for fractional-slot concentrated-winding variable magnetomotive-force memory motor," *IEEE Trans. Power Electron.*, vol. 29, no. 9, pp. 4877–4887, Sep. 2014.
[5] J. Jang, M. Humza, and B. Kim, "Design of a variable-flux permanent-magnet synchronous motor for adjustable-speed operation," *IEEE Trans. Ind. Appl.*, vol. 52, no. 4, pp. 2996–3004, Jul./Aug. 2016.
[6] T. Fukushige, N. Limsuwan, T. Kato, K. Akatsu, and R. D. Lorenz, "Efficiency contours and loss minimization over a driving cycle of a variable-flux flux-intensifying interior permanent magnet machine," *IEEE Trans. Ind. Appl.*, vol. 51, no. 4, pp. 2984–2989, Jul. 2015.
[7] M. Ibrahim, L. Masisi, and P. Pillay, "Design of variable flux permanent-magnet machine for reduced inverter rating," *IEEE Trans. Ind. Appl.*, vol. 51, no. 5, pp. 3666–3674, Sep./Oct. 2015.
[8] B. S. Gagas, K. Sasaki, A. Athavale, T. Kato, and R. D. Lorenz, "Magnet temperature effects on the useful properties of variable flux pm synchronous machines and a mitigating method for magnetization changes," *IEEE Trans. Ind. Appl.*, vol. 53, no. 3, pp. 2189–2199, May/Jun. 2017.
[9] A. Athavale, K. Sasaki, B. S. Gagas, T. Kato, and R. D. Lorenz, "Variable flux permanent magnet synchronous machine (VF-PMSM) design methodologies to meet electric vehicle traction requirements with reduced losses," *IEEE Trans. Ind. Appl.*, vol. 53, no. 5, pp. 4318–4326, Sep./Oct. 2017.
[10] Y. Gong, K. T. Chau, J. Z. Jiang, C. Yu, and W. Li, "Analysis of doubly salient memory motors using preisach theory," *IEEE Trans. Magn.*, vol. 45, no. 10, pp. 4676–4679, Oct. 2009.
[11] C. Yu and K. T. Chau, "Design, analysis, and control of DC-excited memory motors," *IEEE Trans. Energy Convers.*, vol. 26, no. 2, pp. 479–489, Jun. 2011.
[12] C. Yu, S. Niu, S. L. Ho, W. Fu, and L. Li, "Hysteresis modeling in transient analysis of electric motors with AlNiCo magnets," *IEEE Trans. Magn.*, vol. 51, no. 3, Mar. 2015, Art. no. 7300804.
[13] X. Zhu, L. Wang, Y. Chen, L. Chen, and L. Quan, "A non-rare-earth doubly salient flux controllable motor capable of fault-tolerant Control," *IEEE Trans. Magn.*, vol. 51, no. 11, Nov. 2015, Art. no. 8111204.
[14] H. Yang *et al.*, "Analysis of on-load magnetization characteristics in a novel partitioned stator hybrid magnet memory machine," *IEEE Trans. Magn.*, vol. 53, no. 6, Jun. 2017, Art. no. 8103404.
[15] H. Yang, H. Lin, J. Dong, J. Yan, Y. Huang, and S. Fang, "Analysis of a novel switched-flux memory motor employing a time-divisional magnetization strategy," *IEEE Trans. Magn.*, vol. 50, no. 2, Feb. 2014, Art. no. 7021004.
[16] H. Yang *et al.*, "Novel high-performance switched flux hybrid magnet memory machines with reduced rare-earth magnets," *IEEE Trans. Ind. Appl.*, vol. 52, no. 5, pp. 3901–3915, Sep./Oct. 2016.
[17] H. Yang *et al.*, "Design synthesis of switched flux hybrid-permanent magnet memory machines," *IEEE Trans. Energy Convers.*, vol. 32, no. 1, pp. 65–79, Mar. 2017.
[18] D. Wu, X. Liu, Z. Q. Zhu, A. Pride, R. Deodhar, and T. Sasaki, "Switched flux hybrid magnet memory machine," *IET Elec. Power Appl.*, vol. 9, no. 2, pp. 160–170, Feb. 2015.
[19] D. Wu, Z. Q. Zhu, A. Pride, R. Deodhar, and T. Sasaki, "Cross coupling effect in hybrid magnet memory machine," in *Proc. 7th IET Int. Conf. Power Electron. Machin. Drives (PEMD)*, Manchester, U.K, Apr. 2014, pp. 1–6.
[20] W. Q. Chu and Z. Q. Zhu, "Average torque separation in permanent magnet synchronous machines using frozen permeability," *IEEE Trans. Magn.*, vol. 49, no. 3, pp. 1202–1210, Mar. 2013.
[21] J. T. Chen and Z. Q. Zhu, "Winding configurations and optimal stator and rotor pole combination of flux-switching PM brushless AC machines," *IEEE Trans. Energy Convers.*, vol. 25, no. 2, pp. 293–302, Jun. 2010.